

## Phase mixing of Alfvén pulses and wavetrains propagating in coronal holes

BY A. W. HOOD, S. J. BROOKS AND A. N. WRIGHT

*School of Mathematics and Statistics, Mathematical Institute,  
University of St Andrews, North Haugh, St Andrews, Fife KY16 9SS, UK*  
(alan@mcs.st-and.ac.uk)

The propagation of Alfvén pulses into an inhomogeneous model of a solar coronal hole is investigated. The algebraic damping of single and bi-polar pulses remains for the leading and trailing pulses as the number of pulses is increased but the decay of the internal pulses returns to the exponential damping of an infinite wavetrain when three pulses or more are present. Thus, wavetrains with most of their energy residing in internal oscillations will be dominated by efficient exponential damping. In contrast, short wavetrains with most of their energy in the leading and trailing pulses will suffer less efficient algebraic damping. The implications of both the damping of these disturbances to the heating of coronal holes and the nonlinear wave pressure to the acceleration of the solar wind are discussed.

**Keywords:** Sun; magnetic fields; coronal heating; wave propagation

### 1. Introduction

Alfvén waves in a uniform plasma are notoriously difficult to dissipate, due to the small values of both the magnetic resistivity and the plasma viscosity. The classical dissipation length-scales are the order of  $10^8$ – $10^{12}$  times the typical wavelengths. However, it is important that the energy contained in Alfvén waves can be released relatively easily in regions of open magnetic field such as coronal holes. By open magnetic field lines in the solar atmosphere, we mean that the magnetic field, observed at the Sun’s photosphere, extends through the chromosphere, the low corona and out into interplanetary space without returning to the Sun’s surface. The plasma within a coronal hole is cooler than the surrounding plasma inside active regions and closed magnetic loops but it is still at a temperature of the order of a million degrees. This is over 100 times hotter than the plasma at the photosphere and it is important to understand how this plasma is heated to such high temperatures. In the open magnetic field structures of coronal holes, the only feasible mechanism is heating due to the dissipation of magnetic disturbances or waves. Also, waves are thought to play an important role in providing an additional acceleration mechanism in the solar wind. The Parker solar wind model (Parker 1958) predicts that the solar wind is driven by the plasma pressure gradient and becomes supersonic beyond the sonic point located at a radius of approximately five times the solar radius. However, recent observations suggest that the sonic point is located at only two solar radii (Axford *et al.* 1999)

and there must be an additional acceleration mechanism required. One possibility is the wave pressure gradient. For magnetic waves of the form  $\mathbf{b} = b_y(x, z, t)\mathbf{e}_y$ , the wave pressure is  $-\nabla b_y^2/2\mu$  averaged in time over a wave period.

Coronal holes are highly inhomogeneous with many high-density coronal plumes showing up in Extreme-ultraviolet Imaging Telescope (EIT) observations onboard the SOlar and Heliospheric Observatory (SOHO) (DeForest *et al.* 2001). These plumes emanate from strong unipolar magnetic sources at the photosphere inside the coronal holes. Slow magnetohydrodynamic (MHD) modes have been detected in plumes (DeForest & Gurman 1998) but there will almost certainly be higher-frequency fast MHD and Alfvén waves present as well. These have not been clearly detected mainly due to a lack of temporal resolution. However, Harrison *et al.* (2002) have presented evidence of Alfvén waves through line broadening. There is a whole new area of *coronal seismology* that is blossoming, but the interpretation of observed oscillations requires a detailed knowledge of how the various wave modes propagate in an inhomogeneous plasma.

Since coronal holes have a low plasma  $\beta$ , there are only two important MHD wave modes, namely fast magnetoacoustic and Alfvén waves. This paper considers only the propagation of linear Alfvénic disturbances in an inhomogeneous plasma and does not consider the coupling to fast modes.

Alfvén waves on a given field line propagate with a group speed that is determined only by the local field strength and plasma density. This important property means that disturbances on individual magnetic fieldlines propagate at their own speed, dependent on either their own particular wavelength or frequency. In a uniform plasma this property is not important. However, if the Alfvén speed is inhomogeneous and varies in the horizontal direction, then Alfvénic disturbances on different field lines will propagate with different speeds. Thus, a coherent disturbance generated on the photospheric boundary will propagate into the corona and rapidly become out of phase with the neighbouring fieldlines (Heyvaerts & Priest 1983). Large perpendicular gradients will build up and eventually they become so large that dissipation becomes important and the disturbances are damped.

The original phase-mixing mechanism involves an infinite wavetrain that is generated by boundary motions (Heyvaerts & Priest 1983) and various situations involving stratification, flux divergence and nonlinearities have been investigated both analytically and numerically by De Moortel *et al.* (1999, 2000), Ruderman *et al.* (1998), Botha *et al.* (2000) and Steinolfson (1985). Other studies have focussed on the time-dependent nature of phase mixing (Cally 1991; Mann *et al.* 1997). The equilibrium is taken as a uniform vertical magnetic field with a structured density profile in the horizontal (perpendicular) direction. This simple model of a coronal hole illustrates the basic properties of wave propagation in a structured plasma and allows for direct comparison with the results presented in Hood *et al.* (2002). Hence,

$$\mathbf{B}_0 = B_0\mathbf{e}_z, \quad \rho = \rho(x). \quad (1.1)$$

Therefore, the Alfvén speed,  $V_A(x)$  defined by  $V_A^2 = B_0^2/\mu\rho$ , varies from field line to field line. The basic result is that, if the boundary oscillates harmonically as  $\sin\omega t$ , then the magnetic field perturbation,  $b_y\mathbf{e}_y$ , behaves as

$$b_y = \sin\left(\omega\left(\frac{t-z}{V_A(x)}\right)\right) \exp\left(-\frac{\eta\omega^2 V_A'^2 z^3}{6V_A^5}\right), \quad (1.2)$$

where  $\eta$  is the magnetic diffusivity,  $V_A'$  is the horizontal derivative of the Alfvén speed and the damping has a strong exponential dependence on height,  $z$ .

Only a few authors have considered the case of a spatially localized Alfvén wavetrain. Tsiklauri *et al.* (2001) considered small-amplitude Alfvénic disturbances in a low-beta plasma. They investigated the weakly nonlinear generation of fast waves and showed that there is an optimal value of the Alfvén speed gradient for maximal generation. Tsiklauri & Nakariakov (2002) investigated the three-dimensional evolution of a linear Alfvén pulse and found that compressible effects influence the phase-mixing process.

However, Hood *et al.* (2002) have shown that the damping process is slower when an individual pulse is generated, the damping rate being algebraic rather than exponential. The shape of a single pulse rapidly transforms into a travelling Gaussian profile of the form

$$b_y = \frac{1}{\sqrt{1 + V_A'^2 \eta z^3 / 3\sigma^2 V_A^5}} \exp \left[ \frac{-(t - z/V_A)^2}{2(\sigma^2 + V_A'^2 \eta z^3 / 3V_A^5)} \right], \quad (1.3)$$

as discussed in Hood *et al.* (2002). This gives an algebraic decay with height as  $z^{-3/2}$  rather than the exponential decay of the form  $\exp(-z^3)$  for the infinite wavetrain. Indeed, they showed that two pulses of opposite sign also decay algebraically but with a higher power law. This bipolar pulse can be thought of as the sum of two single pulses of opposite sign displaced in time by an amount  $t_1$ , where  $2t_1$  is the time between the generation of the peak and trough at the photospheric boundary. Thus, defining

$$f = \sqrt{\frac{1 + V_A'^2 \eta z^3}{3\sigma^2 V_A^5}},$$

the bipolar pulse can be represented by

$$b_y = \frac{1}{f} \left( \exp \left[ -\frac{(t - z/V_A + t_1)^2}{2\sigma^2 f^2} \right] - \exp \left[ -\frac{(t - z/V_A - t_1)^2}{2\sigma^2 f^2} \right] \right). \quad (1.4)$$

Expanding the square in the exponential and collecting terms together gives

$$b_y = \frac{1}{f} \exp \left[ -\frac{\xi^2/2 - t_1^2}{2\sigma^2 f^2} \right] \left( \exp \left[ -\frac{t_1 \xi}{\sigma f} \right] - \exp \left[ \frac{t_1 \xi}{\sigma f} \right] \right), \quad (1.5)$$

where  $\xi = (t - z/V_A)/\sigma f$ . Finally, the exponentials in the last bracket are expanded in a Taylor series for small  $t_1 \xi/\sigma$  to give

$$b_y = -\frac{2t_1}{\sigma f^2} \xi \exp(-\frac{1}{2}\xi^2),$$

in agreement with the Hermite polynomial solution presented in Hood *et al.* (2002). The maxima and minima occur at  $\xi = \pm 1$  and the amplitudes decay as  $z^{-3}$ , rather than  $z^{-3/2}$  for a single pulse.

Presumably, if a large number of pulses are generated, then the decay rate will return to the exponential case of the infinite harmonic wavetrain. It is an aim of this paper to investigate how the algebraic decay rate is transformed into the exponential decay as the number of pulses is increased.

In this paper, we investigate how the results for a single pulse are modified when more and more pulses are considered. This will allow us to understand how these standard results fit in with the results for the infinite wavetrain. The basic equations are presented and the numerical results described in §2. The decay rates depend on the number of pulses considered and an analytic description is presented in §3. The results and conclusions are discussed in the last section.

## 2. Pulse propagation

In this paper the inhomogeneous Alfvén speed is defined as

$$V_A(x) = 1 + 0.5 \cos(\pi x), \quad (2.1)$$

so that the largest gradient of  $V_A$  is  $V_A' = \frac{1}{2}\pi$  and occurs at  $x = 0.5$ , where  $V_A(0.5) = 1$ . As the pulses propagate away from the lower boundary, where they are generated, large horizontal gradients build up around the region where the gradient of the Alfvén speed is largest. The horizontal gradients continue to build-up until dissipation becomes important and the disturbances are damped. This removal of magnetic energy from the disturbances takes the form of ohmic heating.

The linearized Alfvén wave equation in an inhomogeneous plasma is

$$\frac{\partial^2 b_y}{\partial t^2} = V_A^2(x) \frac{\partial^2 b_y}{\partial z^2} + \eta \frac{\partial}{\partial t} \frac{\partial^2 b_y}{\partial x^2}, \quad (2.2)$$

where  $b_y$  is the perturbed magnetic field component corresponding to an Alfvénic disturbance. A discussion of this equation, the terms neglected and the validity of the coronal hole model is given in Hood *et al.* (2002). The behaviour of the phase mixing of several pulses is illustrated for dissipation due to resistivity. However, all the conclusions are the same if viscosity is considered. The dissipated wave energy will produce viscous heating instead of ohmic heating but the magnitude of the heating is the same.

As we are eventually interested in comparing with the infinite wavetrain results, the disturbances are generated through imposed motions on the lower boundary. This is different to Hood *et al.* (2002) and results in a minor modification to the analytical method. Thus, initially

$$b_y(x, z, 0) = \frac{\partial b_y}{\partial t}(x, z, 0) = 0, \quad (2.3)$$

and the lower boundary condition is

$$b_y(x, 0, t) = F(t). \quad (2.4)$$

If we continue the driving process, then we set  $F(t) = \sin(\omega t)$  in order to reproduce the infinite wavetrain results. However, with the numerical simulation we are able to track the initial transient behaviour before the final steady state is reached. Otherwise, the driving function,  $F(t)$ , will determine the number of pulses that are generated by the boundary motions.

Numerical simulations are carried out using a particular form for the boundary forcing function,  $F(t)$ . To investigate any transient behaviour and to retrieve the

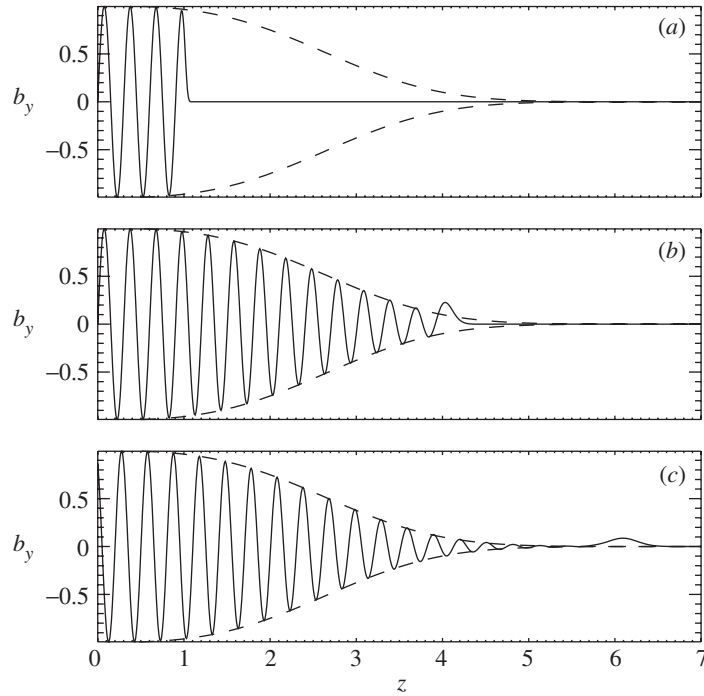


Figure 1. The magnetic field disturbances,  $b_y(0.5, z, t)$ , due to harmonically driven boundary motions are shown as a function of height at different times (a)  $t = 1.0$  s, (b)  $t = 4.0$  s, (c)  $t = 6.0$  s. In all cases the parameters are  $\eta = 10^{-4}$  and  $\omega = 20\pi/2$ . The Heyvaerts & Priest exponential, cubic damping envelope of steady-state phase mixing is shown by the dashed curves.

steady state for an infinite wavetrain, we consider the case

$$F(t) = \begin{cases} \sin^2 \omega t, & 0 \leq t < \frac{\pi}{2\omega}, \\ \sin \omega t, & \frac{\pi}{2\omega} \leq t < \frac{(2n-1)\pi}{2\omega}, \\ \sin^2 \omega t, & \frac{(2n-1)\pi}{2\omega} \leq t < \frac{n\pi}{\omega}, \\ 0, & t > \frac{n\pi}{\omega}. \end{cases} \quad (2.5)$$

The initial and final  $\sin^2 \omega t$  terms are included to ensure that the pulses are smoothly switched on and off. This smoothing process is necessary for the numerical code but can be ignored for the analytical work. The initial state is given by (2.3). The disturbances are generated at the lower boundary and they propagate into the corona. In the region where the Alfvén speed gradient is zero, there is no phase mixing and the waves maintain their harmonic shape with only a minimal amount of damping. However, in the region where the Alfvén gradient is non-zero, phase mixing occurs and the pulses begin to be damped. The behaviour at  $x = 0.5$  is shown in figure 1. Here the magnetic field disturbances as functions of height are shown for different times. The local Alfvén speed is unity and the leading edge has reached the approximate

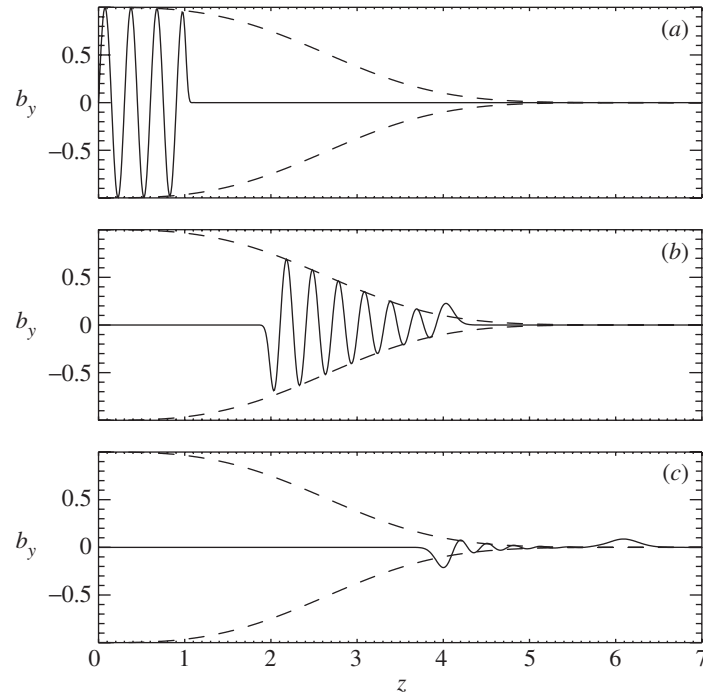


Figure 2. Seven cycles are generated at the boundary and the resulting disturbances are shown as a function of height at  $x = 0.5$  for various times (a)  $t = 1.0$  s, (b)  $t = 4.0$  s, (c)  $t = 6.0$  s. The parameters are  $\eta = 10^{-4}$  and  $\omega = 20\pi/2$ . The exponential, cubic damping of phase mixing is shown by the dashed curves.

height  $z = t$ . This is only approximate since, due to diffusion, the leading edge is now slightly ahead of  $z = t$ . Note that the maximum of the leading pulse does not decay as rapidly as the remaining waves and after a time of approximately four Alfvén times (a value dependent on the particular value of  $\eta$  selected and the form of the boundary forcing function) the leading transient behaviour begins to emerge from the wavetrain. The remaining waves are damped and follow the classical exponential phase-mixing damping (the dashed curves in figure 1), with the damping rate proportional to the cubed power of the height, as found by Heyvaerts & Priest (1983). Only the first half cycle does not follow this exponential damping and, once it has left the remaining waves behind, it forms the Gaussian shape and damps algebraically in the same manner as discussed by Hood *et al.* (2002) for a single pulse.

Once the solitary pulse has left the system, the remaining waves follow the usual steady-state solution for phase-mixed harmonic waves. Presumably, if the driving function is eventually switched off, then there will be a trailing transient pulse as well. This is investigated in the next section. Note that the steady-state solution predicts the exponential cubic damping with height and that this form of damping occurs for all pulses, except the leading one, regardless of the height or time.

#### (a) Several harmonic pulses

Consider the case when there are *seven* cycles of the harmonic driver on the boundary. Thus, the driving function is  $F(t)$ , given by (2.5) for  $t > 0$  and  $t < 14\pi/\omega$ .

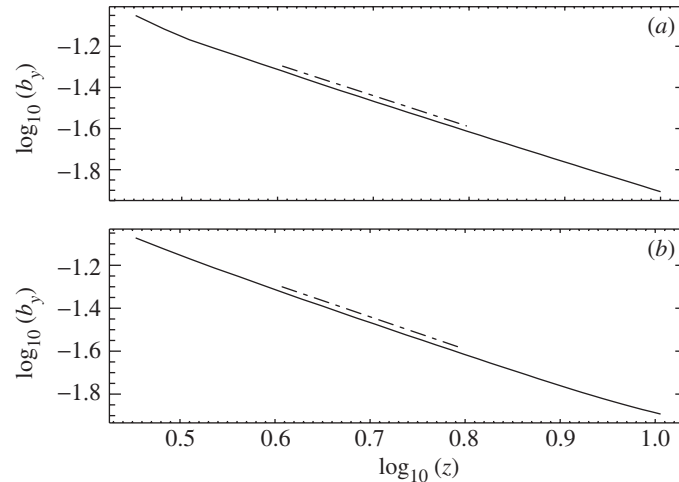


Figure 3. The decay rates,  $z^{-3/2}$ , for the (a) leading and (b) trailing pulses, once they have separated from the wavetrain. As the two pulses are of the same sign, the predicted final decay rate is  $z^{-3/2}$  once they finally interact. This final interaction, which is not shown, occurs after a time  $t = 20$ , when the leading pulse has reached a height of  $z = 20$ .

The behaviour of the waves is shown at  $x = 0.5$  as a function of height in figure 2 for several different times. Note that the damping of the internal waves follows the exponential damping of the infinite wavetrain but there are leading and trailing pulses that take the form of individual Gaussians. When, all the internal waves have damped, these two pulses are initially distinct. However, they eventually spread and interact to form the bipolar pulse shape that was described in Hood *et al.* (2002), although the amplitudes are small by this stage for the example shown in figure 2.

The single-pulse results of Hood *et al.* (2002) can be retrieved by considering a driving of seven-and-a-half cycles.

The decay of the internal pulses follows the exact exponential damping of the infinite wavetrain. In fact, the internal pulses are given exactly by a single sinusoidal function and, hence, they phase mix as if they are part of an infinite harmonic wavetrain with the rapid exponential damping. This is clearly seen in figure 2.

The leading and trailing pulses seen in figure 2 are longer lived and appear to decay at a slower rate. From figure 3, it is clear that they decay algebraically with a power law of the form  $z^{-3/2}$ , as long as the leading and trailing pulses do not interact. However, once they do interact, the decay rate switches to a power law of  $z^{-3}$  if the leading and trailing pulses are of opposite sign (as in figure 2) and they return to  $z^{-3/2}$  if they are of the same sign.

Whether this exponential decay for the internal pulses is a general result or whether it depends on the number of pulses generated and their shape is not clear at present. To answer this, several simulations were generated with a varying number of pulses.

#### (i) Amplitude decay rate

To determine if the decay rate of the internal pulses is always exponential, we investigated the effect of the number of pulses. The leading and trailing pulses always seem to decay algebraically as explained above. Perhaps surprisingly, the internal pulses all

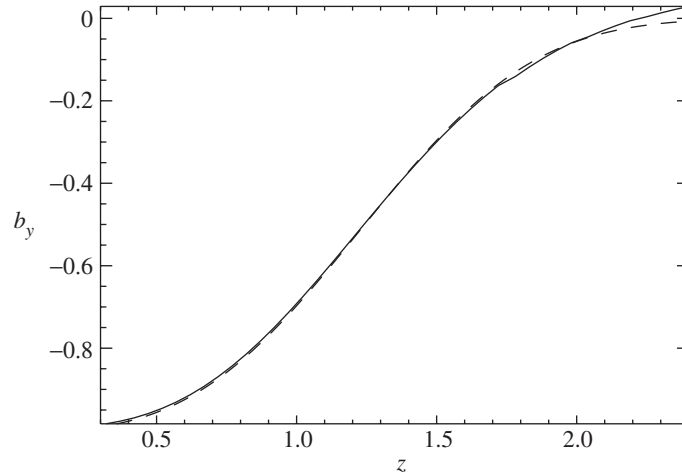


Figure 4. The decay of  $b_y$  for the single internal pulse is shown as a function of height as a solid curve. The dashed curve is the Heyvaerts & Priest exponential curve and in this case  $\eta = 2 \times 10^{-3}$ .

seem to have an exponential decay region that is exactly predicted by the Heyvaerts & Priest expression. This is clearly illustrated in figure 4, where there are only one-and-a-half cycles generated on the boundary, giving a leading and trailing pulse and only one internal pulse. Even for this case the internal pulse decays exponentially. Remembering that the leading and trailing pulses have the same sign, the central value of  $b_y$  will eventually become positive as these pulses combine into one Gaussian pulse. This accounts for the appearance of the positive values at larger heights.

(ii) *Variation of  $\eta$*

The main influence of the resistivity,  $\eta$ , is in the variation of the diffusion length-scale. Remembering that the width of an individual pulse increases as  $\eta^{1/2}z^{3/2}$ , as shown in equation (1.3), it is clear that a decrease in the value of  $\eta$  means that the pulses must propagate to a greater height before the exponential damping can occur. It takes longer for an initial general shape to transform into the internal sinusoidal form. This is clearly illustrated in the following section.

### 3. Analytic theory

(a) *Fourier integral solution*

Using a Fourier integral approach we can obtain an analytical solution for certain wavetrain profiles. The advantage of an analytical solution lies in the fact that we can determine the physical processes behind the various stages of propagation of several pulses. The dependence on the equilibrium properties is clearly illustrated in a way that a numerical solution cannot provide. Consider the initial case of § 2 when a disturbance of  $\sin \omega t$  is started at  $t = 0$ . Thus, the boundary condition at  $z = 0$  can be expressed as a Fourier integral of the form

$$\sin \omega t = \frac{1}{2\pi} \int_{-\infty}^{\infty} a(\tilde{\omega}) e^{i\tilde{\omega}t} d\tilde{\omega}, \quad t > 0,$$

where

$$a(\tilde{\omega}) = \int_0^\infty \sin \omega t e^{-i\tilde{\omega}t} dt = \frac{i\pi}{2} (\delta(\tilde{\omega} + \omega) - \delta(\tilde{\omega} - \omega)) + \frac{1}{2} \left( \frac{1}{\tilde{\omega} + \omega} - \frac{1}{\tilde{\omega} - \omega} \right).$$

Here  $\delta(x)$  is the Dirac delta function and  $i = \sqrt{-1}$ . Taking a Fourier transform of the Alfvén wave equation, we can obtain the Heyvaerts & Priest solution for the transform,  $\bar{b}_y$ , as

$$\bar{b}_y(x, z, \tilde{\omega}) = a(\tilde{\omega}) \exp \left\{ -\frac{i\tilde{\omega}z}{V_A(x)} \right\} \exp \left\{ -\frac{\tilde{\omega}^2 \eta (V'_A)^2 z^3}{6V_A^5} \right\}.$$

Taking the inverse Fourier transform we obtain the final solution in terms of error functions,  $\text{erf}(x) = \int_0^x e^{-u^2} du$ , a diffusion time-scale,

$$t_d = \sqrt{\frac{\eta \omega^2 (V'_A)^2 z^3}{6V_A^5}}, \tag{3.1}$$

and a propagating coordinate  $\xi = \omega(t - z/V_A)$ , as

$$b_y = \frac{1}{4} e^{-t_d^2} \left( 2 \sin(\xi) - i e^{i\xi} \text{erf} \left( it_d + \frac{\xi}{2t_d} \right) - i e^{-i\xi} \text{erf} \left( it_d - \frac{\xi}{2t_d} \right) \right). \tag{3.2}$$

Note that the leading exponential terms correspond to the exponential damping predicted by Heyvaerts & Priest.

The following expansions for the error functions are useful (Abramowitz & Stegun 1970). If  $\xi/2t_d \gg t_d$ , then

$$\text{erf} \left( \frac{\xi}{2t_d} + it_d \right) \approx \text{erf} \left( \frac{\xi}{2t_d} \right) + it_d \exp \left\{ -\frac{\xi^2}{2t_d^2} \right\},$$

$\text{erf}(+\infty) = 1$  and  $\text{erf}(-\infty) = -1$ . On the other hand, if  $\xi/2t_d \ll t_d$ , then

$$\text{erf} \left( it_d + \frac{\xi}{2t_d} \right) \approx \text{erf}(it_d) + \frac{\xi}{2t_d} e^{t_d^2}.$$

Finally, for a general complex number  $\zeta$ , if  $|\zeta| \gg 1$ , then

$$\text{erf}(\zeta) = 1 - \frac{1}{\sqrt{\pi}\zeta} e^{-\zeta^2}.$$

Using these expressions we can approximate  $b_y$ , for small  $z$ , or equivalently small  $t_d$ , as

$$b_y \approx \frac{1}{2} e^{-t_d^2} \sin \omega t \left( 1 + \text{erf} \left( \frac{\omega t}{t_d} \right) \right).$$

For  $t < 0$  the error function tends to  $-1$  and  $b_y \rightarrow 0$ . For  $t > 0$  the error function tends to  $+1$  and  $b_y \rightarrow e^{-t_d^2} \sin(\omega t)$ . Note that the solution will initially follow the exponential damping predicted by Heyvaerts & Priest.

The equivalent expressions for large  $t_d^2 + \xi^2/4t_d^2$  and  $\xi > 0$  give

$$b_y = e^{-t_d^2} \sin(\xi) + \frac{1}{2} \frac{t_d}{\xi^2/4t_d^2 + t_d^2} e^{-\xi^2/4t_d^2}.$$

In a similar manner, if  $\xi < 0$ , then

$$b_y = \frac{1}{2} \frac{t_d}{\xi^2/4t_d^2 + t_d^2} e^{-\xi^2/4t_d^2}.$$

Note how the Gaussian shape automatically appears when the argument of the error function is large. This is in agreement with the numerical results presented in §2. For  $t_d$  small, the solution behaves like  $\sin(\omega t)$  for  $t > z/V_A(x)$  and zero for  $t < z/V_A(x)$ . The sinusoidal term is damped in the exponential manner predicted by Heyvaerts & Priest. However, this term rapidly decreases, and the remaining term is the final Gaussian profile that decays algebraically as found by Hood *et al.* (2002).

(b) *Finite wavetrain*

The effect of a finite wavetrain is investigated now by considering the boundary condition at  $z = 0$  as

$$b_y(x, 0, t) = \begin{cases} \cos \omega t, & -\frac{5\pi}{2\omega} < t < \frac{5\pi}{2\omega}, \\ 0, & \text{elsewhere,} \end{cases}$$

and there are two and a half cycles (or three positive and two negative pulses). Following the Fourier transform approach, the solution can be written as

$$b_y(x, z, t) = \frac{1}{4} e^{-t_d^2} \left( e^{i\xi} \left( \operatorname{erf} \left( it_d + \frac{\xi + 5\pi/2}{2t_d} \right) - \operatorname{erf} \left( it_d + \frac{\xi - 5\pi/2}{2t_d} \right) \right) + \text{c.c.} \right), \quad (3.3)$$

where c.c. stands for complex conjugate. The extra error functions, compared with (3.2), correspond to the switching off of the waves.

The amplitude of the central pulse is given by setting  $\xi = 0$ . It is clear that this portion of the waves decays exponentially, as predicted by Heyvaerts & Priest, while  $2t_d < \frac{5}{2}\pi$ .

It is instructive to relate the diffusion time to a diffusion length by  $l_d(z) = V_A t_d(z)$ . Physically, this corresponds to the length over which the solution has spread out and influenced neighbouring parts of the wave. For example, a delta function will evolve as a Gaussian of width  $l_d$ , and it is often useful to think of a solution as a sum of such functions. In terms of the diffusion length, the above condition for the exponential decay of the central section requires that the diffusion length is smaller than the half-width of the wavetrain. After this height, at which all the pulses have started to interact with each other, the imaginary part of the argument in the error function starts to dominate. The leading behaviour of the difference in the two error functions gives a growing exponential term that cancels with the decaying exponential term outside the brackets in (3.3). The algebraic decay term remains and, at  $\xi = 0$ , takes the form

$$b_y = \frac{10\sqrt{\pi}t_d}{(5\pi/2)^2 + 4t_d^4}.$$

This is valid for large values of  $t_d$  and, in this limit, the amplitude decays as  $t_d^{-3} \propto z^{-3/2}$ , as expected.

From this example it is clear that the exponential decay occurs for the central pulse if there are at least three pulses, two positive and one negative.

#### 4. Discussion and conclusions

The results of Hood *et al.* (2002) showed how an isolated Alfvén pulse would rapidly transform into a travelling Gaussian pulse, with an amplitude that decayed algebraically with height. On the other hand, Heyvaerts & Priest (1983) showed that a harmonically driven system decayed much faster, with an amplitude decay given by an exponential depending on the cube of the height. So there is clearly a connection between these results as the number of pulses increases from a single one to an infinite wavetrain.

In this paper, we showed how the leading transient of a sinusoidal wavetrain rapidly transformed into the predicted Gaussian pulse, while the remaining waves were damped according to the Heyvaerts & Priest result. A finite wavetrain generated a leading and trailing pulse and, while the internal pulses damped exponentially, these remaining pulses behaved as individual Gaussians until they spread out and began to interact. The final behaviour depended on whether the leading and trailing pulses were of the same sign or opposite sign. If they were of the same sign, they combined into a single Gaussian and, if they were of the opposite sign, they behaved like the bipolar pulse discussed in Hood *et al.* (2002).

Interestingly, the internal pulses always decayed with the exponential form of Heyvaerts & Priest. Part of the reason for this is due to the fact that the disturbances were dominated by the particular frequency of the sinusoidal form chosen. What will happen to more general disturbances? If a general pulse is repeated  $n$  times, then the power of the Fourier transform of the signal will be dominated by two main peaks. One peak will be around the period of the individual pulse,  $\tau_p$  (and its higher harmonics) and the other will be around the lifetime of the  $n$  pulses,  $n\tau_p$ . Each individual pulse will transform, in a typical time  $t_d$ , into the particular sinusoidal wavetrain given by the dominant frequency in the Fourier transform. This time-scale,  $t_d$ , is determined by the diffusion time-scale (3.1), which is approximately the time taken for diffusion to influence one pulse in our wavetrain. After  $t_d$ , all the internal pulses will decay at a rate following the Heyvaerts & Priest exponential form, while the leading and trailing pulses will transform into individual travelling Gaussian pulses. Finally, the remaining two Gaussian pulses will interact after each has diffused a distance comparable with the width of the original wavetrain, approximately  $nt_d$ .

The implications for coronal holes are now briefly discussed. Hood *et al.* (1997) showed that the location of the maximum ohmic and viscous dissipation for an infinite wavetrain is at a height,  $z_{\max} = (2V_A^5/\eta\omega^2(V_A')^2)^{1/3}$ . De Moortel *et al.* (1999, 2000) showed that this height depended on gravitational stratification and the area divergence of the magnetic field. However, it is possible for the maximum heating to occur at a height of 1.4 solar radii. The finite number of pulses behaves in a very similar manner. The main energy deposition of the internal pulses is deposited around the same height, for the dominant Fourier component. The higher-frequency components are damped lower down and the lower-frequency components higher up. However, the energy contained in the leading and trailing pulses is relatively small and is unlikely to contribute significantly to the heating. A key point, discussed in De Moortel *et al.* (1999), is that all the energy injected into the corona through the Poynting flux at the photospheric base (integrated over the lifetime of all the pulses) is dissipated by phase mixing.

The infinite wavetrain contributes to a non-zero, time averaged wave pressure,  $b_y^2/2\mu$ , which provides an additional acceleration to the solar wind. Using the Heyvaerts & Priest solution, this is proportional to  $\exp(-\eta\omega^2(V'_A)^2 z^3/3V_A^5)$ . The maximum of the vertical pressure gradient is located at the same height as the maximum of the ohmic heating. For the parameters chosen by De Moortel *et al.* (2000), the maximum of the wave pressure gradient is at a realistic height. For a finite number of pulses, there is a non-zero wave pressure at a fixed height, but it only exists for a finite time during the passage of the pulses. The variation of this wave-pressure force with height will again depend on the power contained within each of the individual Fourier components. A more complete theory requires the solution of the nonlinear MHD equations and is beyond the scope of this paper.

### Appendix A. Rectangular wavetrains

An analytical solution, using a train of  $n$  rectangular pulses, illustrates how the evolution of a wavetrain of a more arbitrarily shaped pulse will evolve on three distinct time-scales. Firstly, the arbitrary pulses will become smoother without any apparent amplitude decay. This occurs on a time-scale that is related to the width of the individual pulses. Secondly, the rapid exponential decay for the internal pulses will occur on the time-scale predicted by Heyvaerts & Priest. The leading and trailing pulses do not exhibit this rapid decay. Finally, the leading and trailing pulses decay on a time-scale related to the width of the original wavetrain.

Since the perturbations have been generated by boundary motions that have a substantial symmetry (and hence a substantial contribution from a single Fourier frequency), this symmetry remains during the subsequent evolution. Consider a positive half cycle in the internal structure of our wavetrain and the neighbouring negative half cycle. If these pulses are antisymmetric about the zero point, then the diffusion of the positive pulse into the negative pulse exactly balances the diffusion of the negative part into the positive part. Hence, the zero point will remain at the same place. This will also happen with all the internal pulses. Hence, the internal zeros remains the same distance apart and the structure rapidly evolves towards the sinusoidal function that matches these zeros. All the internal pulses behave as if they are part of an infinite sinusoidal wavetrain and they are damped exponentially in the usual phase-mixing manner.

To illustrate this with a non-sinusoidal driver, take

$$b_y(x, 0, t) = - \sum_{j=-n}^n (-1)^j \left( U\left(\frac{t + (2j + 1)}{\omega}\right) - U\left(\frac{t + (2j - 1)}{\omega}\right) \right),$$

where the Heaviside function  $U(t)$  is defined by

$$U(t) = \begin{cases} 1, & t > 0, \\ 0, & t < 0. \end{cases}$$

Using the Fourier transform method above, the solution is

$$b_y(x, z, t) = \frac{1}{2} \sum_{j=-n}^n (-1)^j \left( \operatorname{erf}\left(\frac{\xi + (2j + 1)/\omega}{2t_d}\right) - \operatorname{erf}\left(\frac{\xi + (2j - 1)/\omega}{2t_d}\right) \right). \quad (\text{A } 1)$$

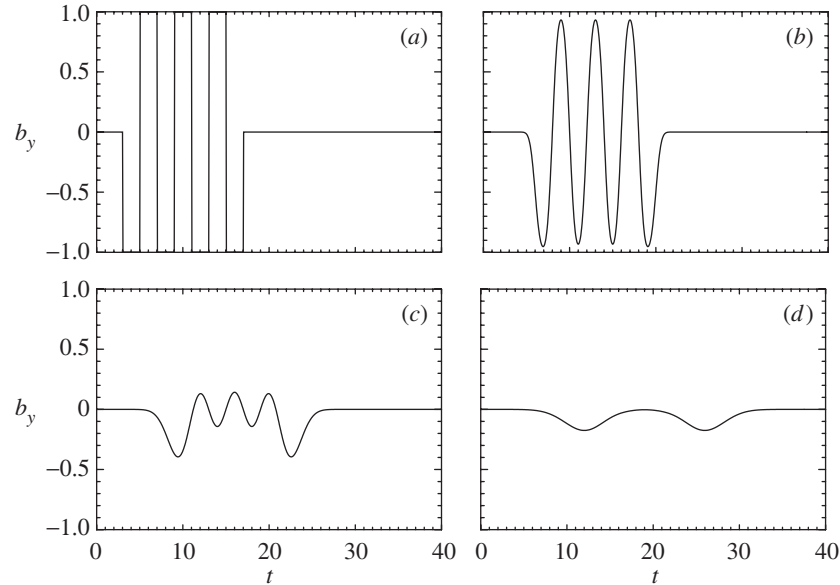


Figure 5. The evolution of the rectangular wavetrain is shown as a function of time,  $t$ , at  $x = 0.5$  for the heights (a)  $z = 0$ , (b)  $z = 3$ , (c)  $z = 6$ , (d)  $z = 9$ . The sharp edges of the pulse smooth quickly before the amplitude rapidly decays.

Diffusion converts the square edges into a rounded sinusoidal shape in a time related to the diffusion time across an individual pulse. Recalling that  $t_d = \eta\omega^2(V'_A)^2 z^3 / 6V_A^5$ , setting  $2t_d = 1$  and rearranging for the height  $z$ , our estimate of the height at which the pulses assume a sinusoidal shape is

$$z = \left( \frac{3V_A^5}{\eta\omega^2(V'_A)^2} \right)^{1/3} = 3.7.$$

Of course, this is equivalent to requiring that  $l_d$  be equal to internal pulse width. Here, for illustration, we have used  $\omega = \pi/2$ ,  $\eta = 10^{-2}$ ,  $V'_A = \pi/2$  and  $V_A = 1$ , in keeping with the results shown in figure 5. In addition, the time when the exponential decay finishes will be approximately when the diffusion time is of the order of the duration of the complete signal, i.e. the diffusion length is of the order of the width of the wavetrain. Hence,  $2t_d = 2n$ . Using the above values, we have

$$z = 7.9.$$

As an example, consider the case with  $n = 5$ .  $b_y$  as a function of time, at  $x = 0.5$  is shown for various heights in figure 5.

The square shape of the pulses disappeared by the time the pulses reached a height of  $z = 2.4$  and the central pulses completely disappeared once the pulses reached  $z = 8.7$ . These are comparable with the simple estimates obtained in terms of the diffusion lengths and times.

To understand how this evolution occurs, consider the Fourier transform of the solution. A power spectrum as a function of  $z$  and frequency is shown in figure 6.

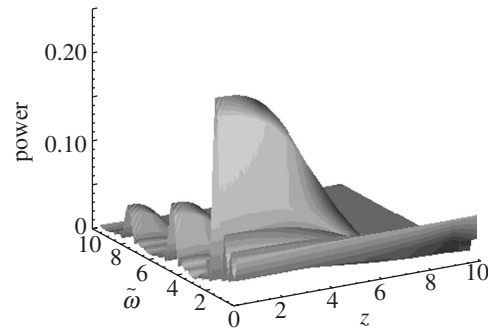


Figure 6. The power spectrum of the magnetic field perturbations for the imposed temporal boundary condition as a function of  $z$  and frequency,  $\tilde{\omega}$ .

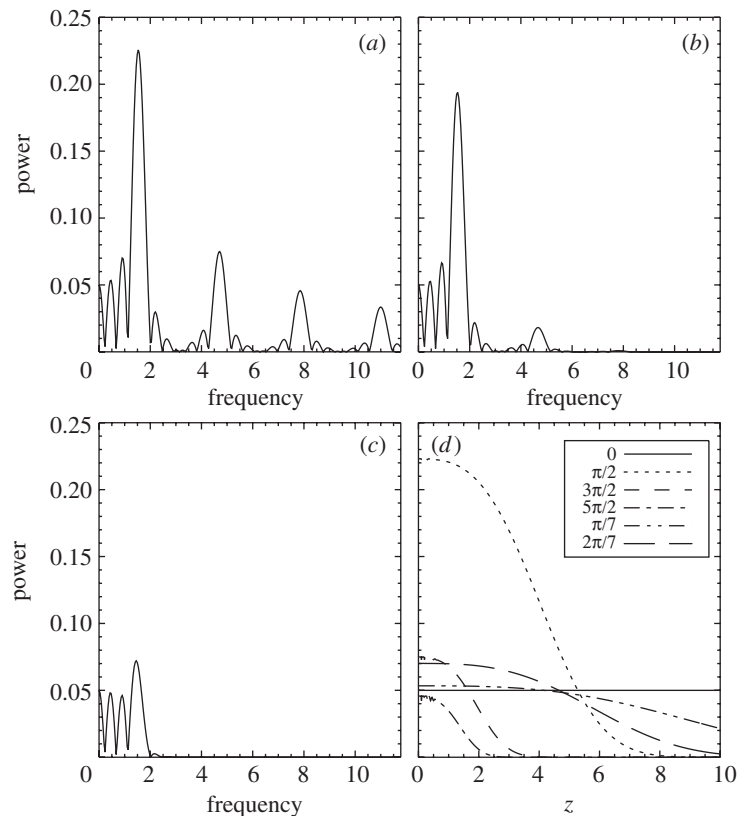


Figure 7. Three slices through the surface shown in figure 6 at (a)  $z = 0$ , (b)  $z = 2.5$  and (c)  $z = 5.0$ . (d) Variation with  $z$  at selected frequencies (see text for details).

At  $z = 0$  there are clear peaks in power around  $\tilde{\omega} = \pi/2, 3\pi/2$  and  $5\pi/2$  (see figure 7). Since the period of the internal pulses is four in this case, the dominant frequency is  $2\pi/4 = \pi/2$ . The higher harmonics are associated with the higher-frequency components present in the Fourier transform of the square wavetrain. Indeed, the signal can be thought of in terms of a superposition of sinusoidal signals,

and the Heyvaerts & Priest solution describes how the amplitude of each component should decay with  $z$  in figure 6 (see equation (1.2)).

To demonstrate the varying decay rates more clearly, figure 7 displays several slices through the surface in figure 6 at increasing height. The final panel shows the variation of amplitude with  $z$  at the frequencies  $\pi/2$  (dotted line),  $3\pi/2$  (short-dashed line),  $5\pi/2$  (dot-dashed line) which are associated with the shape of the square wave, and 0 (solid line),  $\pi/7$  (triple-dot-dashed line) and  $3\pi/7$  (long-dashed line) which are related to the leading and trailing pulses. These smaller values of  $\tilde{\omega}$  can also be thought of as related to the total time that the boundary is driven, namely  $2\pi/14 = \pi/7$ .

From the Heyvaerts & Priest solution (1.2), the exponential damping with height depends on the square of the frequency so that the power at the higher frequencies rapidly disappears with height. Consider the evolution of the central pulse, corresponding to  $\xi = 0$ . Now the variations of  $b_y(0.5, z, t)$ , where  $z = V_A t$  as  $\xi = 0$ , can be considered by using the Heyvaerts & Priest result applied to each Fourier component. The higher frequencies, large values of  $\tilde{\omega}$ , will decay faster with  $z$  than the dominant mode at  $\pi/2$ . This means that the individual pulse will rapidly transform, on a time-scale related to the diffusion time,  $t_d$ , into the sinusoidal form that is related to the zeros of the initial pulse. The solution will now decay exponentially until the amplitude of the Fourier component at  $\pi/2$  becomes comparable in size to the Fourier components with smaller values of  $\tilde{\omega}$ . Once the low frequencies begin to dominate, the subsequent decay will be slower and the Fourier transform approaches  $4(\sin \tilde{\omega}/\tilde{\omega}) \exp(i\tilde{\omega}(t - z/V_A))$  for large  $z$ . Inverting this transform gives the travelling Gaussian profile of Hood *et al.* (2002), which decays relatively slowly (algebraically, not exponentially) with  $z$ .

The numerical simulations were carried out on the UKMHD JREI/SHEFC funded parallel computer at St Andrews University. The authors thank the Particle Physics and Astronomy Research Council for financial support. Thanks to Tony Arber for suggesting that the Fourier transform might give a simple analytical solution.

## References

- Abramowitz, M. & Stegun, I. 1970 *Handbook of mathematical functions*. New York: Dover.
- Axford, W. I., McKenzie, J. F., Sukhorukova, G. V., Banaszekiewicz, M., Czechowski, A. & Ratkiewicz, R. 1999 Acceleration of the high speed solar wind in coronal holes. *Space Sci. Rev.* **87**, 25–41.
- Botha, G. J. J., Arber, T. D., Nakariakov, V. M. & Kennan, F. P. 2000 A developed stage of Alfvén wave phase mixing. *Astron. Astrophys.* **363**, 1186–1194.
- Cally, P. S. 1991 Phase-mixing and surface-waves: a new interpretation. *J. Plasma Phys.* **45**, 453–479.
- DeForest, C. E. & Gurman, J. B. 1998 Observation of quasi-periodic compressive waves in solar polar plumes. *Astrophys. J.* **501**, L217–L220.
- DeForest, C. E., Plunkett, S. P. & Andrews, M. D. 2001 Observation of polar plumes at high solar altitudes. *Astrophys. J.* **546**, 569–575.
- De Moortel, I., Hood, A. W., Ireland, J. & Arber, T. D. 1999 Phase mixing of Alfvén waves in a stratified and open atmosphere. *Astron. Astrophys.* **346**, 641–651.
- De Moortel, I., Hood, A. W. & Arber, T. D. 2000 Phase mixing of Alfvén waves in a stratified and radially diverging, open atmosphere. *Astron. Astrophys.* **354**, 334–348.

- Harrison, R. A., Hood, A. W. & Pike, C. D. 2002 Off-Limb EUV line profiles and the search for wave activity in the low corona. *Astron. Astrophys.* **392**, 319–327.
- Heyvaerts, J. & Priest, E. R. 1983 Coronal heating by phase-mixed shear Alfvén waves. *Astron. Astrophys.* **117**, 220–234.
- Hood, A. W., Ireland, J. & Priest, E. R. 1997 Heating of coronal holes by phase mixing. *Astron. Astrophys.* **318**, 957–962.
- Hood, A. W., Brooks, S. J. & Wright, A. N. 2002 Coronal heating by the phase mixing of individual pulses propagating in coronal holes. *Proc. R. Soc. Lond. A* **458**, 2307–2325.
- Mann, I. R., Wright, A. N. & Hood, A. W. 1997 Multiple-timescales analysis of ideal poloidal Alfvén waves. *J. Geophys. Res.* **102**, A2, 2381–2390.
- Parker, E. N. 1958 Dynamics of the interplanetary gas and magnetic fields. *Astrophys. J.* **128**, 664–676.
- Ruderman, M., Nakariakov, V. & Roberts, B. 1998 Alfvén wave phase mixing in two-dimensional open magnetic configurations. *Astron. Astrophys.* **338**, 1118–1124.
- Steinolfson, R. S. 1985 Resistive wave dissipation on magnetic inhomogeneities: normal-modes and phase mixing. *Astrophys. J.* **295**, 213–219.
- Tsiklauri, D. & Nakariakov, V. M. 2002 A three dimensional Alfvénic pulse in a transversely inhomogeneous medium. *Astron. Astrophys.* **393**, 321–329.
- Tsiklauri, D., Arber, T. D. & Nakariakov, V. M. 2001 A weakly nonlinear Alfvénic pulse in a transversely inhomogeneous medium. *Astron. Astrophys.* **379**, 1098–1105.